

Structural and Electronic Study of an Amorphous MoS₃ Hydrogen-Generation Catalyst on a Quantum-Controlled Photosensitizer**

Ming L. Tang, David C. Grauer, Benedikt Lassalle-Kaiser, Vittal K. Yachandra, Lilac Amirav, Jeffrey R. Long, Junko Yano, and A. Paul Alivisatos*

Dedicated to the Fritz Haber Institute, Berlin, on the occasion of its 100th anniversary

The design and synthesis of catalysts, especially for the production of solar fuels, is a major challenge in developing sources of renewable energy.^[1,2] Catalyst development requires an understanding of the mechanism(s) involved and the nature of the active site.^[3,4] While platinum group metals have unrivalled activity for both hydrogen and oxygen evolution,^[5,6] they are scarce and expensive. Photocatalytic systems relying on earth-abundant materials are therefore desirable for large scale energy production.^[7,8] Herein, we examine the structure and electronic properties of an amorphous molybdenum sulfide species and its possible use for photocatalytic hydrogen evolution. The catalyst was grown on a seeded quantum-rod sensitizer, a model system for investigating the photophysics of solar fuel generation. This catalyst's activity is shown experimentally to be associated with under-coordinated molybdenum centers, and we document that a reduced form of MoS₃ is an active species for hydrogen generation.

Molybdenum sulfides are prevalent in both biological enzymes and industrial catalysts. Mo metalloenzymes are involved in carbon, nitrogen, and sulfur metabolism, while synthetic molybdenum sulfides serve as industrial hydro-treating catalysts^[9–12] and are proven electrocatalysts for the

hydrogen evolution reaction (HER). MoS₂,^[13,14] incomplete cubane [Mo₃S₄]⁴⁺ clusters,^[15,16] molecular molybdenum catalysts,^[17,18] and amorphous MoS₂ made by a reduction of MoS₃^[19] have been shown to be active HER catalysts. Highly active HER catalysts, including Pt, have a Gibbs free energy of H adsorption (ΔG_{H}) close to zero.^[14] Density functional theory calculations show that the equatorial sulfur atoms in Fe–Mo cofactors in nitrogenase enzymes as well as the bridging S atom on the edge sites of MoS₂ bind H atoms with $\Delta G_{\text{H}} \approx 0$.^[14] These calculations, coupled with scanning tunneling microscopy (STM) studies, have indicated that molybdenum sulfide based hydrodesulfurization and HER catalysts derive their activities from under-coordinated atoms. Recent investigations of MoS₂ nanoparticles using STM combined with electrochemical measurements have revealed that HER activity scales with the number of edge sites, rather than nanoparticle area, adding substantial evidence that under-coordination is critical to activity.^[13]

There is also substantial current interest in molecularly thick and structurally disordered metal oxide and sulfide layers supported on electrodes, surfaces, and nanoparticles as potential catalysts for the HER^[19] and oxygen evolution reaction^[20] (OER). Such ultrathin films can support a variety of unusual and possibly favorable bonding geometries and may retain flexibility in healing and recovering.^[20,21] Despite their potential, such systems remain very difficult to characterize, impeding reproducibility and the communication of results between groups. Mechanisms are difficult to pin down when structural and electronic characterization is lacking.

In this work, we use X-ray absorption techniques to obtain structural information on a catalytically active disordered molybdenum chalcogenide species that was grown on a well-controlled seeded quantum rod photosensitizer system with very high surface area. The high surface area of the colloidal system enables us to employ a variety of X-ray characterization techniques. Yet the system is also well-defined: Amorphous layers of MoS₃ are deposited on quantum-controlled photosensitizers. We take advantage of recent work showing that cadmium chalcogenide nanocrystals can be engineered to systematically control the separation of photo-generated holes and electrons,^[22–25] thus allowing us to modulate the photochemical yield of hydrogen.^[26]

Nanorods of CdS grown on CdSe seeds with varying diameters and pure CdS nanorods of differing length were synthesized by a seeded-growth method previously reported.^[24] These particles have been of interest as a model system for investigating photochemical HER because their

[*] Dr. M. L. Tang,^[†] D. C. Grauer,^[†] Dr. L. Amirav, Prof. J. R. Long, Prof. A. P. Alivisatos
 Department of Chemistry, University of California, Berkeley
 Material Sciences, Lawrence Berkeley National Laboratory (LBNL)
 Berkeley, CA 94720 (USA)
 E-mail: alivis@berkeley.edu
 jyano@lbl.gov

Dr. B. Lassalle-Kaiser, Dr. V. K. Yachandra, Dr. J. Yano
 Physical and Biosciences
 LBNL, Berkeley, CA 94720 (USA)

[†] These authors contributed equally to this work.

[**] We thank Chris Chang for use of his microwave. The photocatalysis experiments were supported by the Helios Solar Energy Research Center, while nanocrystal work was supported by the Physical Chemistry of Semiconductor Nanocrystals Program, KC3105. TEM studies were performed at the National Center for Electron Microscopy at LBNL. The above centers and programs were supported by the Office of Science, Office of Basic Energy Sciences (OBES) of the U.S. Department of Energy (DOE) under Contract No. DE-AC02-05CH11231. Synchrotron facilities were provided by the Stanford Synchrotron Radiation Laboratory (SSRL) operated by DOE OBES.



Supporting information (experimental details) for this article is available on the WWW under <http://dx.doi.org/10.1002/anie.201104412>.

bandgap and band offsets are appropriate for driving water splitting with a single photon, and the ability to control the pathways of charge migration offers additional means for making more stable photocatalysts.^[23] A sampling of these monodisperse, high-quality and crystalline nanorods is shown in Figure 1 b. The pseudo-type II heterojunction in the CdSe/

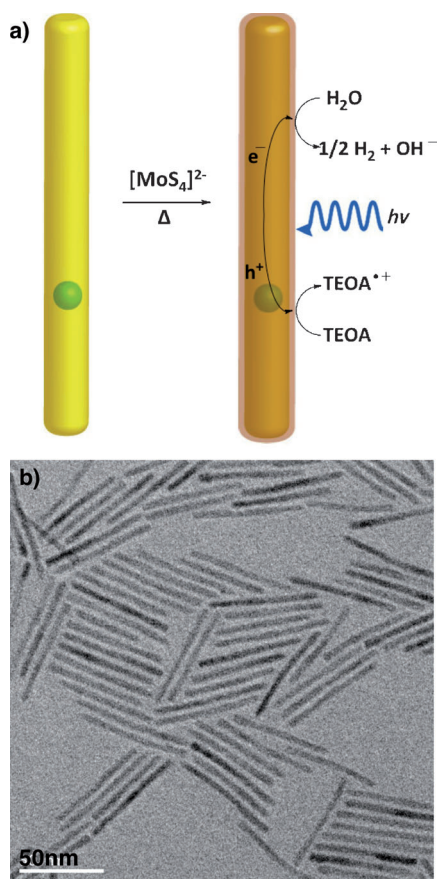


Figure 1. a) MoS_3 deposition on a CdSe-seeded CdS nanorod, with photocatalytic hydrogen production in the visible range using triethanolamine (TEOA) as a sacrificial reductant. b) Bright-field TEM image of CdSe-seeded CdS nanorods (length 60 nm). The scale bar is 50 nm.

CdS nanorod heterostructure results in a photogenerated hole that is spatially confined to the core and an electron that can delocalize over the entire structure. This inhomogeneous spatial distribution, a result of the staggered band alignments from CdSe and CdS that are controlled with the seed and rod diameters, decreases electron–hole overlap and increases the exciton lifetime as the rod length increases or the seed diameter decreases.^[25]

A one-step thermal process was used to deposit an amorphous molybdenum sulfide film from $(\text{NH}_4)_2\text{MoS}_4$ on the nanorods. In comparison, previous work involving cadmium chalcogenide photosensitizers decorated with MoS_2 cocatalysts involved either bulk CdS modified by high-temperature calcinations under H_2S ^[27] or quantum-confined CdSe structures functionalized by high-power ultrasonication.^[28] Following the synthesis of the seeded rods, the nanorods coated with octadecylphosphonic acid (ODPA)

were dissolved in toluene and mixed with *o*-dichlorobenzene and an aliquot of $(\text{NH}_4)_2\text{MoS}_4$ dissolved in *N*-methylpyrrolidone, as shown schematically in Figure 1 a. The mixture was then subjected to microwave heating at 90°C for 50 min (details are provided in Table S1 in the Supporting Information, SI), after which the initially hydrophobic yellow-orange nanorod solution acquired a brown color and a marked solubility in water. UV/Vis absorption of the as-synthesized rods and those modified by this thermal deposition exhibit the same excitonic transitions and energies (Figure S1, SI), indicating that no etching of the CdS rods, nor deposition of MoS_2 , which has an absorption associated with its bandgap of ca. 1040 nm, has occurred. In transmission electron microscope (TEM) micrographs, we do not observe preferential deposition of a molybdenum sulfide species on the tips of the rods under these conditions. These results taken together are consistent with the thermal deposition of a surface coating on the rods.

After the thermal deposition step, the rods were precipitated and resuspended in acetonitrile to remove any excess dissolved Mo species not physically attached to the rod. This step was repeated again, after which 0.05–0.10 nmol of rods were suspended in a 5.0 mL solution of 0.1 M Tris buffer (pH 7.0; Tris = tris(hydroxymethyl)aminomethane) and 0.2 mL of triethanolamine (TEOA) at room temperature. Deposition of this thin film results in a photochemically active system for hydrogen generation. Control experiments with as-synthesized CdSe/CdS nanorods showed negligible rates of H_2 production under the photocatalytic conditions employed here. Irradiation of a solution of $(\text{NH}_4)_2\text{MoS}_4$ or MoS_3 in water under the same conditions gave no hydrogen either. Therefore we conclude that intimate contact between the MoS_3 surface layer and the nanorods is vital for efficient charge transfer. Pure CdS dots and rods have activities that are, at best, a half of the seeded rods, highlighting the importance of the lengthened exciton lifetime in improving catalytic activity. Activities of $100 \text{ mmol h}^{-1} \text{ g}^{-1}$ of H_2 are obtained using MoS_3 -coated 60 nm CdS rods containing 2.8 nm CdSe seeds, with apparent quantum efficiencies (AQEs) of 10% using 450 nm light. This efficiency is comparable to a similar system with Pt cocatalysts on the tips of the same rods, which displays AQEs of 20% using the same light source.^[26] This system ($100 \text{ mmol h}^{-1} \text{ g}^{-1}$) has a far higher activity than found in previous studies of photocatalytic H_2 formation from crystalline MoS_2 photosensitized by cadmium chalcogenides. The activity of bulk CdS/ MoS_2 was $5.3 \text{ mmol h}^{-1} \text{ g}^{-1}$,^[27] and that of CdSe/ MoS_2 nanoribbons was $0.89 \text{ mmol h}^{-1} \text{ g}^{-1}$.^[28] Though AQEs would serve a better comparison, those studies did not report values for quantum efficiencies.

The MoS_3 -coated nanocrystals have from 1 to 4 Mo ions deposited for every Cd ion on the surface of the nanorod, as measured by inductively coupled plasma-optical emission spectroscopy (ICP-OES). The volume and surface area of each nanorod was estimated from TEM images (for length) and UV/Vis spectra (for diameter)—details are in the SI. The amorphous nature of this coating can be seen in Figure S2a (SI); following deposition, the powder X-ray diffraction (XRD) pattern shows no additional reflections, while high-

resolution TEM (Figure S2b, SI) gives only lattice fringes arising from CdS planes.

Figure 2a shows X-ray photoelectron spectroscopy (XPS) data of the Mo-coated rods before and after catalysis. The binding energy of the Mo 3d_{5/2} (Mo 3d_{3/2}) feature at 229.9 eV (233.0 eV) suggests that the oxidation state of the precatalyst is Mo^V before photocatalysis. Upon photocatalysis, the Mo 3d_{5/2} (Mo 3d_{3/2}) peak is shifted to lower energy at 228.6 eV (231.8 eV), indicating the reduction of Mo^V to Mo^{IV}. This Mo^{IV} state was also observed in the amorphous MoS₃ precatalyst as well as the actual MoS₂ electrocatalysts reported by Merki et al.^[19]

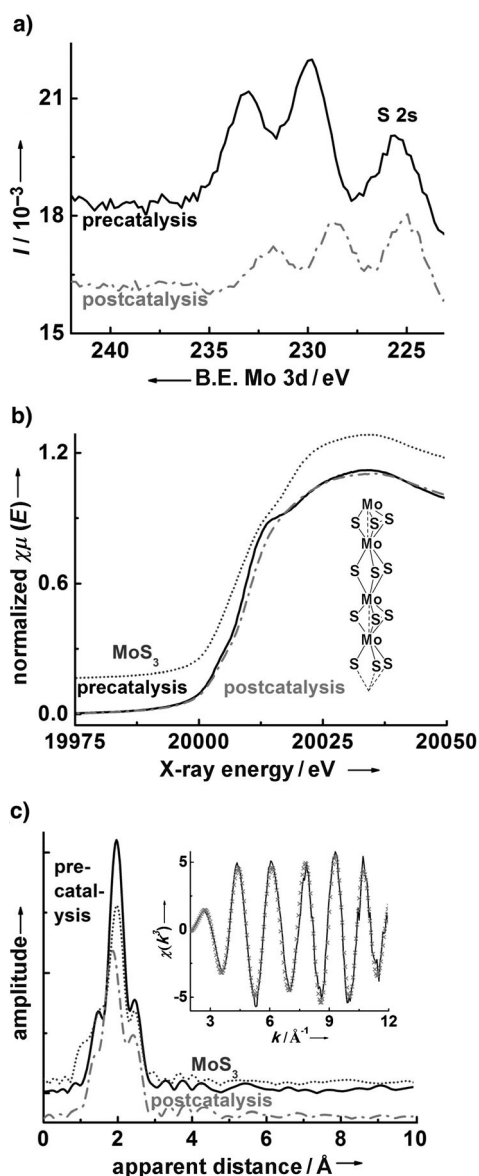


Figure 2. MoS₃-functionalized nanorods before (solid black line) and after catalysis (dotted-dashed gray line). a) XPS data indicating a reduction of the Mo 3d binding energy during photocatalysis. b) Mo K-edge XANES spectra for MoS₃ (inset: structure) and MoS₃-functionalized nanorods before and after catalysis. c) Mo EXAFS spectra for MoS₃- and MoS₃-functionalized nanorods before and after catalysis. Inset: fit of MoS₃ (gray crosses) to the pre-catalysis sample (solid line). Note the decrease in Mo–S nearest neighbor distance following catalysis.

The Mo K-edge X-ray absorption near edge structure (XANES) and extended X-ray absorption fine structure (EXAFS) spectra of the Mo-coated rods before and after catalysis are shown in Figure 2 b,c. In the XANES spectrum, the rising edge energy is shifted to higher energies (+1.0 eV) after catalysis, accompanied by a change in shape. Although the XANES energy is often used as an indicator of the metal oxidation state, it is difficult to interpret spectra particularly when the reaction is accompanied by changes in ligand environment. For the formal oxidation state of Mo, we therefore rely on the XPS result (Figure 2 a), which is a direct indicator of the metal binding energy. The XANES and EXAFS of the Mo-coated rods are compared with spectra of crystalline MoS₂, MoS₃, (NH₄)₂MoS₄ model compounds (Figure S3a,b, SI), and truncated cubane [Mo₃S₄]⁴⁺ clusters.^[29] Based on the differences in Mo–S and Mo–Mo distances, MoS₂, (NH₄)₂MoS₄, and [Mo₃S₄]⁴⁺ can clearly be ruled out as structural analogues for the molybdenum sulfide coating on the nanorods. On the other hand, the EXAFS spectrum is strikingly similar to that of MoS₃,^[30,31] suggesting that the Mo photocatalyst is analogous to the MoS₃ motif. The curve fitting^[32–34] result of the Mo-coated rod before catalysis is shown in Figure 2 c (inset). The Mo–S and Mo–Mo distances prior to photocatalysis are (2.44 ± 0.01) Å and (2.78 ± 0.02) Å, respectively (Table S2, SI). These distances are identical to those found in bulk MoS₃. After photocatalysis, the Mo–S distance decreases to (2.35 ± 0.02) Å, and the average coordination number (number of sulfur ligands per molybdenum) becomes less than 6. For Mo–Mo interactions seen as a shoulder at R' = 2.45 Å in the EXAFS spectra (Figure 2 c), distances and the number of interactions remain the same before and after catalysis. Alternatively, this peak could be due to the Mo–Cd interactions or a mixture of Mo–Mo and Mo–Cd interactions as we expect Mo to be bridged to Cd by sulfide bonds. However, Mo–Cd interactions may not be observed if distances are long (> 4 Å) or if there is a large distribution of Mo–Cd distances, which can arise from an incoherent interface between wurtzite CdS and the amorphous MoS₃. Neutron diffraction^[35], XPS^[36,37] and EXAFS^[30] data suggest that MoS₃ forms linear chains of face-sharing MoS₆ octahedra with the chemical formula of Mo^{IV}(S²⁻)(S₂²⁻) or Mo^V(S²⁻)₂(S₂²⁻)_{1/2} (Figure 2 b, inset).

The reduction of the Mo centers coupled with a contraction in Mo–S bond length upon catalysis, suggests a modification in the bridging disulfide bond that is proposed for the structure of MoS₃. A reduction of this bond would donate more electron density into the Mo–S bonding orbitals and result in the shortening of the Mo–S bonds observed in EXAFS, as well as the reduction of the Mo center observed by XPS. The bridging nature of the disulfide unit may be altered, each bridging sulfur becoming a terminal protonated thiolate ligand. This would account for the lower coordination number determined from fits for post-catalysis samples. These structural changes can account for the 30–50 min induction period observed in all of our samples before hydrogen generation commences (Figure 3 a). The fact that our catalyst is an amorphous molybdenum sulfide which undergoes a photoreduction prior to catalysis marks a similarity to work by Merki et al.^[19] They report an electrochemical reduction of

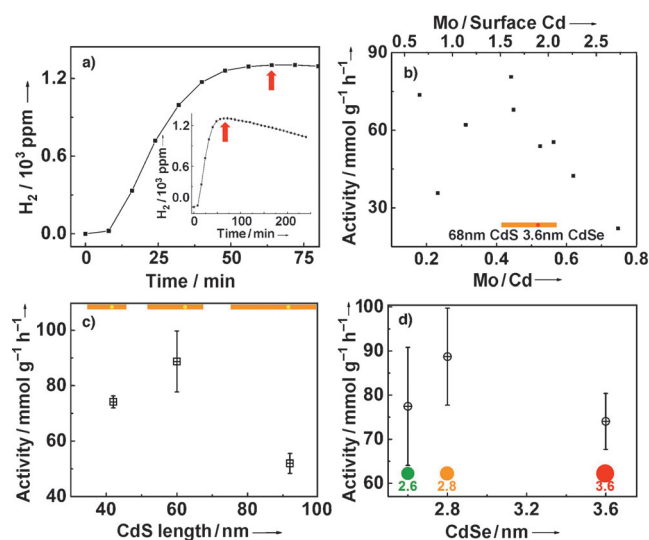


Figure 3. a) A typical gas chromatogram observed for a MoS₃-coated CdS/CdSe nanorod using 450 nm light with an induction period of approximately 50 min. 0.07 nmol of rods were used with 5.0 mL 0.1 M tris buffer (pH 7.0) and 0.20 mL TEOA. The inset shows the measurement over a period of four hours. The activities are derived from the maximum rate of H₂ produced, as indicated by the arrows. b) Maximum photocatalytic activity (mmol H₂ g⁻¹ h⁻¹) correlated with surface MoS₃ coverage for 68 nm CdS/3.6 nm CdSe (orange bar/red circle). c) Activity correlated with the CdS nanorod length (orange bars) for a 2.8 nm CdSe seed (yellow circles). d) Activity for different CdSe seed sizes in a 65 nm CdS nanorod. (c) and (d) show an average of 3 data points.

MoS₃ to form MoS₂ as the active species. However, both the pre-catalyst and actual catalyst here structurally resemble MoS₃. Both crystalline and amorphous MoS₂ have a Mo–Mo interaction at 3.2 Å.^[38] We do not observe this scattering feature at 3.2 Å in the EXAFS of any of our samples. Thus we conclude that a reduced form of MoS₃ is the active catalyst in our system.

Given this picture of the catalyst film, we can now return to a study of the photocatalytic activity as a function of the nanorod variables by examining a series of seeded rods with different seed sizes and rod lengths. Figure 3b plots the overall activity for 68 nm long CdS rods incorporating a 3.6 nm CdSe seed versus Mo/Cd surface coverage and absolute Mo/Cd ratio. Surface Mo compositions correlated with activity for all other heterostructure dimensions are given in Figure S4 (SI). The activities are extracted from the maximum rate of production of hydrogen, as given by the gas chromatogram (Figure 3a). For all the heterostructures, the optimum Mo/surface Cd ratio ranges from 0.7:1–2.0:1. When the Mo/Cd ratio is too high, light absorption by the CdS nanorod is inhibited by the coating itself. To extract the dependence on seed size, a series of rods approximately 65 nm in length were grown with 2.6, 2.8, and 3.6 nm CdSe seeds; for the dependence on rod length, 42, 60, and 92 nm long rods were synthesized with a 2.8 nm CdSe seed. The TEM images and UV/Vis spectra of these rods are shown in Figure S5 (SI).

Photocatalytic H₂ production depends strongly upon nanorod length. As shown in Figure 3c, for rods of different length with the same 2.8 nm CdSe seed, the highest activity is observed for 60 nm rods, followed by the 42 nm rods and then the 92 nm rods. We can understand these results by recognizing that the presence of the seed acts to separate photo-generated electron–hole pairs, with the hole remaining localized in the seed, while the electron is largely delocalized. The effect of the seed only extends over a finite length, however. While the longest rods may absorb more light, there is an increased probability of direct absorption in the CdS-only region, and the photogenerated electron–hole pair may relax or decay by a variety of mechanisms without the hole ever falling into the seed. Excitons generated too far from the seed will not be subject to the staggered band alignments at the interface of the CdSe seed and CdS and hence will not be separated into species which are more available to do work. Conversely, in shorter rods, the excited electron may not delocalize into as large a volume as possible and will have more wavefunction overlap with the localized hole, resulting in a truncated excitonic lifetime. This argument implies an ideal length, which we observe at 60 nm. This optimum length also appears in some of our previous work, where Pt tips were used as the H₂-producing cocatalyst with the same seeded rods.^[26]

Comparing seeds of different size with rods of approximately the same length (ca. 65 nm) in Figure 3d, we see that large seeds of 3.6 nm perform relatively poorly. This is because large (>3.5 nm) CdSe seeds only weakly confine photogenerated electrons, so their conduction band energy approaches the bulk value, which lies significantly below the conduction band energy of the quantum-confined CdS. With this band offset between the two materials, the electron cannot delocalize significantly into the CdS portion of the rod. This results in the electron and hole wavefunctions overlapping substantially to produce a shortlived exciton.

The decrease in H₂ production over time is attributed to the gradual dissolution of MoS₃ from the surface of the rods. Even in the absence of light, 2–20% of the starting Mo content is found in solution after 5 h. This dissolution is also seen in the incomplete cubane [Mo₃S₄]⁴⁺ clusters.^[15,16] ICP-OES measurements conducted on the supernatant and a pellet of the MoS₃-coated nanorods exposed to photocatalytic conditions revealed only Mo, with no Cd in solution. This decomposition is not accelerated by light. The unstable nature of this surface coating of MoS₃ is consistent with an incoherent interface between the trigonal prismatic MoS₃ and wurtzite CdS nanorod. Work towards a self-healing catalyst^[20] is being pursued.

To close, our system consists of an amorphous MoS₃ surface coating on semiconductor nanocrystals that is photocatalytically active for H₂ evolution. Comprised of colloiddally synthesized, earth-abundant and inexpensive materials, it produces H₂ with visible light, with a maximum activity of 100 mmol H₂ h⁻¹ g⁻¹ and AQE of 10% at λ = 450 nm. During the induction period, the initial MoS₃ pre-catalyst is photo-reduced to form an under-coordinated species structurally similar to MoS₃, distinct from MoS₂. This reduced MoS₃ catalyst is shown for the first time to be active for HER.

Received: June 25, 2011
Revised: August 11, 2011
Published online: September 28, 2011

Keywords: hydrogen · molybdenum · nanoparticles · photochemistry · X-ray absorption spectroscopy

- [1] M. S. Dresselhaus, I. L. Thomas, *Nature* **2001**, *414*, 332.
[2] N. S. Lewis, D. G. Nocera, *Proc. Natl. Acad. Sci. USA* **2006**, *103*, 15729.
[3] M. G. Walter, E. L. Warren, J. R. McKone, S. W. Boettcher, Q. X. Mi, E. A. Santori, N. S. Lewis, *Chem. Rev.* **2010**, *110*, 6446.
[4] X. B. Chen, S. H. Shen, L. J. Guo, S. S. Mao, *Chem. Rev.* **2010**, *110*, 6503.
[5] O. Khaselev, J. A. Turner, *Science* **1998**, *280*, 425.
[6] K. Maeda, T. Takata, M. Hara, N. Saito, Y. Inoue, H. Kobayashi, K. Domen, *J. Am. Chem. Soc.* **2005**, *127*, 8286.
[7] A. Le Goff, V. Artero, B. Jusselme, P. D. Tran, N. Guillet, R. Metaye, A. Fihri, S. Palacin, M. Fontecave, *Science* **2009**, *326*, 1384.
[8] X. C. Wang, K. Maeda, A. Thomas, K. Takanabe, G. Xin, J. M. Carlsson, K. Domen, M. Antonietti, *Nat. Mater.* **2009**, *8*, 76.
[9] R. Prins, V. H. J. Debeer, G. A. Somorjai, *Catal. Rev. Sci. Eng.* **1989**, *31*, 1.
[10] A. Tuxen, J. Kibsgaard, H. Gobel, E. Laegsgaard, H. Topsøe, J. V. Lauritsen, F. Besenbacher, *ACS Nano* **2010**, *4*, 4677.
[11] M. Taniguchi, D. Imamura, H. Ishige, Y. Ishii, T. Murata, M. Hidai, T. Tatsumi, *J. Catal.* **1999**, *187*, 139.
[12] H. Topsøe, B. S. Clausen, F. E. Massoth, *Hydrotreating Catalysis-Science and Technology*, Springer, Berlin, **1996**.
[13] T. F. Jaramillo, K. P. Jorgensen, J. Bonde, J. H. Nielsen, S. Horch, I. Chorkendorff, *Science* **2007**, *317*, 100.
[14] B. Hinnemann, P. G. Moses, J. Bonde, K. P. Jorgensen, J. H. Nielsen, S. Horch, I. Chorkendorff, J. K. Nørskov, *J. Am. Chem. Soc.* **2005**, *127*, 5308.
[15] T. F. Jaramillo, J. Bonde, J. D. Zhang, B. L. Ooi, K. Andersson, J. Ulstrup, I. Chorkendorff, *J. Phys. Chem. C* **2008**, *112*, 17492.
[16] Y. Hou, B. L. Abrams, P. C. K. Vesborg, M. E. Björketun, K. Herbst, L. Bech, A. M. Setti, C. D. Damsgaard, T. Pedersen, O. Hansen, J. Rossmeisl, S. Dahl, J. K. Nørskov, I. Chorkendorff, *Nat. Mater.* **2011**, *10*, 434.
[17] A. M. Appel, D. L. DuBois, M. R. DuBois, *J. Am. Chem. Soc.* **2005**, *127*, 12717.
[18] H. I. Karunadasa, C. J. Chang, J. R. Long, *Nature* **2010**, *464*, 1329.
[19] D. Merki, S. Fierro, H. Vrubel, X. Hu, *Chem. Sci.* **2011**, *2*, 1262.
[20] M. W. Kanan, D. G. Nocera, *Science* **2008**, *321*, 1072.
[21] M. W. Kanan, J. Yano, Y. Surendranath, M. Dinca, V. K. Yachandra, D. G. Nocera, *J. Am. Chem. Soc.* **2010**, *132*, 13692.
[22] D. V. Talapin, R. Koeppel, S. Gotzinger, A. Kornowski, J. M. Lupton, A. L. Rogach, O. Benson, J. Feldmann, H. Weller, *Nano Lett.* **2003**, *3*, 1677.
[23] D. V. Talapin, J. S. Lee, M. V. Kovalenko, E. V. Shevchenko, *Chem. Rev.* **2010**, *110*, 389.
[24] L. Carbone, C. Nobile, M. De Giorgi, F. D. Sala, G. Morello, P. Pomba, M. Hytch, E. Snoeck, A. Fiore, I. R. Franchini, M. Nadasan, A. F. Silvestre, L. Chiodo, S. Kudera, R. Cingolani, R. Krahne, L. Manna, *Nano Lett.* **2007**, *7*, 2942.
[25] A. Sitt, F. Della Sala, G. Menagen, U. Banin, *Nano Lett.* **2009**, *9*, 3470.
[26] L. Amirav, A. P. Alivisatos, *J. Phys. Chem. Lett.* **2010**, *1*, 1051.
[27] X. Zong, H. J. Yan, G. P. Wu, G. J. Ma, F. Y. Wen, L. Wang, C. Li, *J. Am. Chem. Soc.* **2008**, *130*, 7176.
[28] F. A. Frame, F. E. Osterloh, *J. Phys. Chem. C* **2010**, *114*, 10628.
[29] C. E. Hédoire, E. Cadot, F. Villain, A. Davidson, C. Louis, M. Breyse, *Appl. Catal. A* **2006**, *306*, 165.
[30] S. J. Hibble, D. A. Rice, D. M. Pickup, M. P. Beer, *Inorg. Chem.* **1995**, *34*, 5109.
[31] S. P. Cramer, K. S. Liang, A. J. Jacobson, C. H. Chang, R. R. Chianelli, *Inorg. Chem.* **1984**, *23*, 1215.
[32] M. Newville, *J. Synchrotron Radiat.* **2001**, *8*, 322.
[33] M. Newville, B. Ravel, D. Haskell, J. J. Rehr, E. A. Stern, Y. Yacoby, *Phys. B* **1995**, *208*, 154.
[34] J. J. Rehr, R. C. Albers, *Rev. Mod. Phys.* **2000**, *72*, 621.
[35] S. J. Hibble, G. B. Wood, *J. Am. Chem. Soc.* **2004**, *126*, 959.
[36] K. S. Liang, S. P. Cramer, D. C. Johnston, C. H. Chang, A. J. Jacobson, J. P. Deneufville, R. R. Chianelli, *J. Non-Cryst. Solids* **1980**, *42*, 345.
[37] K. S. Liang, J. P. Deneufville, A. J. Jacobson, R. R. Chianelli, F. Betts, *J. Non-Cryst. Solids* **1980**, *35–6*, 1249.
[38] R. I. Walton, A. J. Dent, S. J. Hibble, *Chem. Mater.* **1998**, *10*, 3737.